Particle Accelerators, 1993, Vol. 42(2), pp. 65–79
Reprints available directly from the publisher
Photocopying permitted by license only

DEPENDENCE OF QUADRUPOLE POLE-TIP FIELDS ON BEAM PARAMETERS AND DESIGN OF NONDISPERSIVE OPTICS FOR FINAL-FOCUSING SYSTEMS FOR HIGH-CURRENT HEAVY-ION BEAMS

D. D.-M. HO

Lawrence Livermore National Laboratory, Livermore, CA 94550

K. R. CRANDALL

AccSys Technology, Inc., Pleasanton, CA 94588

(Received 30 March 1992; in final form 19 October 1992)

This paper consists of two parts: First, an approximate scaling law is derived that relates the pole-tip magnetic field of the final-focusing quadrupole to the focal spot size and all the essential heavy-ion beam parameters (current, atomic weight, emittance, charge state, and velocity). Calculations show that this law is reasonably accurate for a useful range of parameters and that it is useful in heavy-ion fusion system studies. Second, a first-order nondispersive focusing system is designed with the space-charge effect properly included. Calculations show that the first-order distortion of the particle distribution from uniformity is not important. It is therefore possible, in principle, to design a nondispersive system to bend high-current beams so that direct line-of-sight neutrons can be avoided.

KEY WORDS: Accelerator Fusion, Heavy-Ion Accelerators, Lattices, Particle Dynamics

1. INTRODUCTION

Heavy-ion accelerators are receiving increased attention as drivers in inertial confinement fusion (ICF)[1] for commercial energy production because they can have a high repetition rate (>> 1 Hz),[2,3] high efficiency (up to 40%),[3] and good reliability over many pulses. An important requirement for a heavy-ion driver is the ability to focus kiloampere beams onto a millimeter-size spot (the typical size of an ICF pellet) using quadrupole magnets. Two aspects of the final focusing system are addressed in this paper.

First, it is useful to have a scaling law for the focusing system for studies of heavy-ion fusion (HIF) systems. Several authors have attempted to obtain such a scaling law. For example, Garren[4] obtained a scaling formula for vacuum chamber propagation, and Lee[5] modeled a focusing system without space-charge effects. In this paper, we derive a scaling law that relates, with reasonable accuracy, the pole-tip magnetic field of the final-focusing quadrupole to the focal spot size and all the parameters (current, atomic

weight, emittance, charge state, and velocity) of a high-current heavy-ion beam. For non-neutralized beams, this law shows that if the beam power on the focal spot is kept fixed, the pole-tip magnetic field increases as the particle mass increases and as the charge state and particle velocity decrease. If the ion-stopping range is fixed, this law allows one to obtain the beam atomic weight that can minimize the pole-tip field.

Second, it is necessary to bend the beam so that direct line-of-sight neutrons can be avoided. Wollnik[6] designed bending magnets for a long focusing system; here, we present the design of bending magnets for a short focusing system. (It is important to keep the length of an HIF focusing system to a minimum because the longitudinal space-change force causes the ends of high-current beams to expand rapidly.[7]) This design is first-order nondispersive, and the effect of space charge is included self-consistently in our calculation. We also conclude that nonlinear electric fields induced by the first-order distortion of particle distribution from uniformity caused by the bending magnets are not important.

This paper is organized as follows: Section 2 gives an example of a typical heavy-ion final focusing system. Then we derive the scaling law and discuss the behavior of the focusing system, according to this law, as we change various parameters. Section 3 discusses the dependence of the pole-tip field on the atomic weight and stopping range of beam particles. Section 4 presents the design of a first-order nondispersive focusing system and discusses the cause and effect of the nonlinear electric field. Section 5 summarizes the results. The appendix gives the ion-stopping formula.

2. DERIVATION OF THE SCALING LAW FOR FINAL-FOCUSING SYSTEMS

Figure 1 shows the configuration of a typical final-focusing system for HIF. This system is designed using the envelope code TRACE[8] for a 10 GeV beam with atomic mass 210, unnormalized emittance 20 mm·mrad, charge state $q = 2$, and a current of 2 kA. The configuration shown here represents a waist-to-waist focusing system (i.e., the envelope has circular cross section and zero slope at the starting point and at the focal spot). At the entrance of the focusing system, the beam waist has a 2.88 cm radius. The beam then undergoes radial expansion due to space-charge force and is finally focused by four large-aperture quadrupoles onto a focal spot with 2.5 mm radius. Table 1 gives the magnetic field gradients and the dimensions of the focusing system. The quadrupoles are numbered Q_1 through Q_4. Four quadrupoles are used because five would make the system too long and three would make the field gradients too high. The drift distance L between the focal spot and the exit plane of the fourth quadrupole is 6 m. This is the reference focusing system referred to throughout the paper. Note that we have made the maximum excursions of the envelope in x and y directions roughly equal; this minimizes the second-order chromatic aberration, the third-order geometric aberration, and the maximum pole-tip magnetic field.

To obtain the scaling law, we first relate the beam envelope radius r_L (at the exit plane of the fourth quadrupole) to the beam parameters and the focal spot radius r_0 using the vacuum envelope equation for uniform-density beams with K-V distribution and with equal emittances and displacements in the two transverse directions. The equation has the form

TABLE 1: Reference system parameters for charge-state-2, 2-kA, 10-GeV beam with atomic weight 210 and unnormalized emittance 20.5 mm·mrad.

Quadrupole number	Magnetic field gradient (T/m)	Quadrupole length (m)	Distance from quadrupole center to waist at entrance (m)
Q_1	-6.29	2.075	15.0375
Q_2	10.10	3.250	19.0000
Q_3	-12.44	3.250	23.4750
Q_4	17.03	1.575	26.8875

$$\frac{d^2r}{ds^2} - \frac{g}{2r} - \frac{\varepsilon^2}{r^3} = 0 \ , \tag{1}$$

where

$$g = 1.278 \times 10^{-7} \frac{qI}{A_b(\beta\gamma)^3} \ .$$

Here r is the beam radius, s is the distance along the direction of propagation, ε is the unnormalized emittance, A_b is the atomic weight of the beam ion, I is the electrical current, q is the charge state, and $\beta\gamma$ is the usual relativistic factor. All units are SI.

Integrating Eq. (1) yields

$$\begin{aligned} \theta^2(L) &\equiv \left(\frac{dr}{ds}\Big|_L\right)^2 \\ &= \varepsilon^2\left(\frac{1}{r_0^2} - \frac{1}{r_L^2}\right) + g\ln\left(\frac{r_L}{r_0}\right) \ . \end{aligned} \tag{2}$$

Since $r_L >> r_0$, we can ignore the $1/r_L^2$ term.

Following Garren,[4] we define $\theta_0 \equiv \varepsilon/r_0$ and replace r_L by $L\theta_0$ in Eq. (2). This approximation is valid since r_L is inside the logarithmic term. For example, for the reference system, $r_L \approx 2L\theta_0$. Therefore, using $L\theta_0$ instead of r_L in Eq. (2) results in only about 10% error in $\theta(L)$. Eq. (2) then becomes

$$\theta(L) \approx \left[\theta_0^2 + g\ln(L\theta_0/r_0)\right]^{1/2} \ . \tag{3}$$

Numerical calculations presented in the following paragraph show that

$$r_L \approx L\theta(L) \ . \tag{4}$$

Substituting the beam parameters for the reference system shown in Fig. 1 into Eq. (4) gives $r_L = 10.1$ cm. This is within 6% of the actual value of $r_L = 9.5$ cm obtained from numerical integration of Eq. (1). [Note that for this example, the space-charge term — the second term inside the bracket in Eq. (3) — is about three times greater than the emittance term, which is the first term inside the bracket]. As the current is

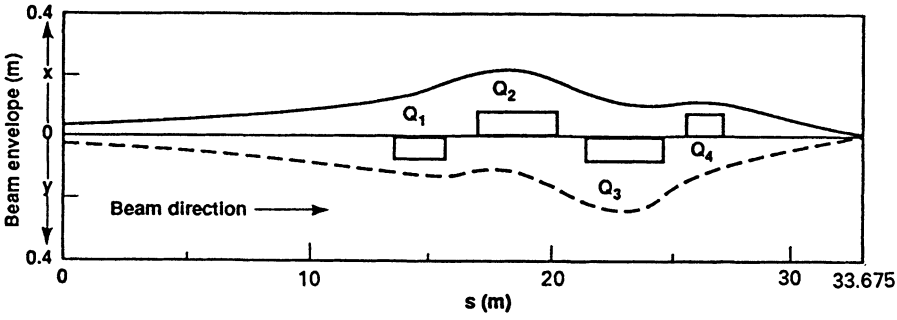

FIGURE 1: Reference final focusing system for a charge-state +2, 2-kA, 10-GeV beam with atomic weight 210 and unnormalized emittance 20.5 mm·mrad. The solid and dashed curves show the envelope in the transverse x and y directions, respectively.

increased to 10 kA, the difference between the values obtained from Eq. (3) and that from numerical integration is still within 6%. However, as the current increases further to 30 kA, the difference becomes greater than 11%. This is because the approximation we made for the logarithmic term is no longer valid for very high current. (Thus, Eq. (4) cannot be used for light-ion beams for which the atomic weight is two orders of magnitude lower and the current is two orders of magnitude higher.) In contrast, for beam propagation with charge neutralization, the space-charge term will become smaller than the emittance term, so Eq. (3) provides an even better approximation of the actual value. For example, when the current decreases to 0.1 kA, the difference between the values obtained from Eq. (3) and that from numerical integration is less than 2%. Eq. (4) is therefore applicable to a wide range of currents at HIF-relevant parameters.

To relate Eq. (4) to the quadrupole pole-tip magnetic field B_p, we model the reference system by a simplified point-to-point configuration (i.e., the envelope has zero radius at the starting point and at the focal spot) with thin lenses, as shown in Fig. 2. The focal length of each lens has the same value L, and the focal length can be expressed as

$$f = \frac{\gamma A_b m_p v}{qeB'\ell_{\text{mag}}} \quad , \tag{5}$$

where B' is the quadrupole field gradient, e is the electronic unit of charge, ℓ_{mag} is the length of the magnet, m_p is the proton mass, and v is the particle velocity. The solid line represents particle trajectory in the x direction (and the dashed line the trajectory in the y direction); initial and final slopes are at angle θ. Space-charge force is not included in this simplified model. This approximation is valid since beam envelope size is large except near the focus and thus space-charge force is not important except near

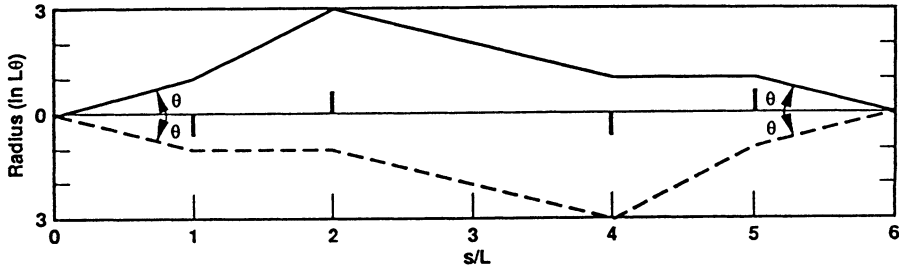

FIGURE 2: Final focusing system modeled by four thin lenses of focal length L (indicated by dark vertical lines). The solid and dashed curves show the envelope in the transverse x and y directions, respectively.

the focus.[9] To relate the beam radius and angle at the exit plane of the fourth quadrupole to the beam parameters, Eqs. (3) and (4) are applied to the drift space.

In Fig. 2, the maximum envelope excusion is $3L\theta$. The pole-tip field is

$$B_p = (3L\theta + \delta)B' \ , \tag{6}$$

where δ is the spacing requirement for neutron shielding between the beam envelope and the magnet. The typical value of δ is 0.1 m; this value will be used throughout this paper.[10] Combining Eqs. (3), (5), and (6), we obtain a relation for B_p for our simplified model:

$$B_p = \frac{cA_b m_p \beta\gamma}{qeL\ell_{\rm mag}} \left\{ 3L \left[\left(\frac{\varepsilon_0}{r_0} \right)^2 + 1.278 \times 10^{-7} \frac{qI}{A_b(\beta\gamma)^3} \ln\left(\frac{L\theta_0}{r_0} \right) \right]^{1/2} + \delta \right\} \ . \tag{7}$$

This functional dependence of B_p on beam parameters should apply to realistic systems as well, since space charge acts mainly near the focus, regardless of the quadrupole structure. However, because of various approximations used in the simplified model from which Eq. (7) was obtained (e.g., quadrupoles are modeled by thin lenses with equal focal strength, and a point-to-point configuration is used), the value of B_p given by Eq. (7) will differ from the actual B_p by some multiplicative factor. To obtain this factor, we compare the value of B_p obtained from Eq. (7) with that obtained from TRACE for the reference system shown in Fig. 1. We have found that the same multiplicative factor applies to systems similar to Fig. 1 for a variety of conditions, as we will show.

In the simplified model shown in Fig. 2, the maximum envelope excursion occurs at both the second and third lenses. However, we need only consider the value of B_p at the third quadrupole, since numerical calculations always show that the third quadrupole has a higher B_p than the second. Using Eq. (7), we find that B_p at the

third quadrupole of the reference system is 2.19 T, whereas $B_p = 4.3$ T from numerical calculation. Thus the scaling law with the correct multiplicative factor is

$$B_p = \frac{1.96 c A_b m_p \beta\gamma}{qeL\ell_{\mathrm{mag}}} \left\{ 3L \left[\left(\frac{\varepsilon_0}{r_0} \right)^2 + 1.278 \times 10^{-7} \frac{qI}{A_b(\beta\gamma)^3} \ln\left(\frac{L\theta_0}{r_0} \right) \right]^{1/2} + \delta \right\} . \tag{8}$$

To check the accuracy of Eq. (8), we compare B_p obtained from Eq. (8) with that obtained from TRACE by varying various beam parameters of the reference system. (When a parameter is varied, all other beam parameters are kept fixed unless stated otherwise.) As the parameters are varied, four constraints are imposed. First, all lengths in the focusing system are the same as in the reference system except the distance between the waist and the entry plane of the first quadrupole. Second, the maximum excursions of the envelope in the x and y directions are adjusted so that they are roughly equal. Third, the beam power on the focal spot [which is proportional to $A_b(I/q)\beta^2$] is kept fixed. Fourth, the beam envelope radius a at the entrance of the focusing system follows the relation

$$a \cong \sqrt{\frac{g}{2\bar{k}_0}} , \tag{9}$$

where the average applied force per unit mass from the magnetic FODO channel[11]

$$\bar{k}_0 \cong \frac{3 - 2\eta}{12} \eta^2 l^2 k_0^2 ,$$

and the usual quadrupole strength constant

$$k_0 = \frac{B'}{[B\rho]} .$$

Here η is the fractional occupancy of quadrupoles, l is the half period of a FODO structure, and $[B\rho]$ is the magnetic rigidity. Eq. (9) is obtained by balancing the space-charge term and the external focusing-force term in the envelope equation with a being the average beam radius in a FODO channel. Emittance term is omitted here since the beam is space-charge dominated in a FODO channel. We assume that B', η, and l remain unchanged when various beam parameters are varied. Consequently,

$$a \propto \sqrt{g/k_0^2} .$$

Under the above constraints, we then vary several parameters, one at a time. The value of A_b is increased from 210 to 420 (corresponding, e.g., to using molecular ions) while decreasing I by a factor of 2 from the reference system to keep the same incoming beam power at the focal spot constant. The emittance is decreased by a factor of 2. The charge state q is decreased from 2 to 1 (so that the current drops by a factor of 2). By reducing the particle velocity from the reference velocity v_0, kinetic energy is

TABLE 2: Values of B_p obtained from Eq. (8) and from TRACE

	B_p from Eq. (8) (T)	B_p from TRACE (T)	Distance between waist and first quadrupole (m)	Waist radius (cm)
Reference system	4.3	4.3	14.0	2.88
Values of parameters under variation from the reference system				
A_b=420(I=1.0 kA)	6.3	6.4	21.5	2.88
ε=10.25 mm·mrad	4.0	3.8	13.0	2.88
q=1(I=1.0 kA)	6.3	6.4	21.5	2.88
K.E. = 5 GeV (v=$v_0/\sqrt{2}$)	6.7	6.8	14.0	3.42
r_0=1.5 mm	4.7	4.7	18.5	2.88
I=1.0 kA	3.5	3.3	16.0	2.04

reduced to 5 GeV and current is increased by a factor of 2. The r_0 is decreased from 2.5 to 1.5 mm, and finally the current is decreased from 2 to 1 kA. (When current varies, the beam power varies accordingly. The total beam power is kept constant by varying the number of beams.) Table 2 gives the value of B_p obtained from Eq. (8) and from TRACE for the focusing system under the variation of the above parameters. The values are within 6% of each other, and thus Eq. (8) provides a reasonably accurate approximation of the focusing system. All the data in Table 2 correspond to focusing the beam onto a 2.5-mm-radius focal spot except when stated otherwise.

Figure 3 shows the behavior of B_p as A_b, ε, q, v^2, r_0, and I vary, as calculated from Eq. (8). Figs. 3(c) and 3(d) indicate that B_p increases as q and v^2 decrease. This is because when q decreases, the efficiency of the quadrupole magnets decreases faster than the space-change force near the focal spot. When kinetic energy v^2 decreases (and current increases in order to keep the beam power constant), the efficiency of the quadrupole magnets decreases and the space-charge force increases. Consequently, B_p increases in both cases.

3. DEPENDENCE OF B_P ON THE ATOMIC WEIGHT AND STOPPING RANGE OF BEAM IONS

One parameter of relevance to HIF is the stopping range R of the target material for the incoming beam, which determines the radiation conversion efficiency.[12] For a fixed R, there exists a relation between B_p and A_b which allows one to minimize B_p by varying A_b. To derive such a relation, we first plot the incoming particle velocity and energy versus A_b for various beam ions, as shown in Fig. 4. The stopping material for Fig. 4 is beryllium at 300 eV with $R = 0.125$ and 0.06 g/cm^2. These curves are plotted using Eq. (A.6), given in the Appendix. For the same stopping range, particle current is increased as A_b decreases so that the beam power is conserved. For example, comparing Pb and Kr ($A_b \cong 210$ and 84, respectively), we see that the velocity for Kr is about

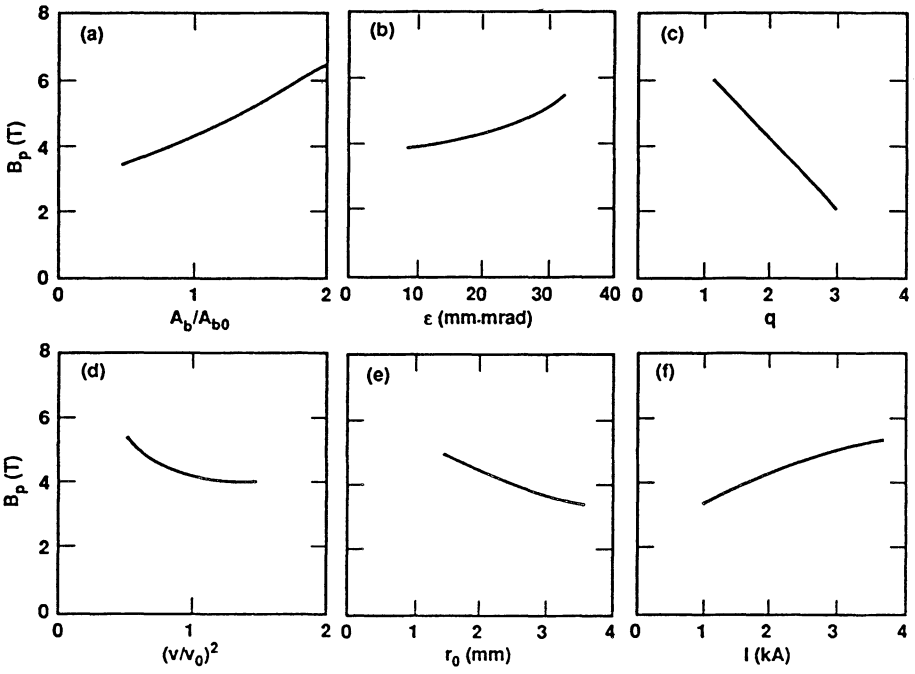

FIGURE 3: Pole-tip magnetic field vs. (a) ratio of beam atomic weight A_b to reference atomic weight A_{b0} (=210); (b) emittance; (c) beam charge state; (d) square of the ratio of the beam velocity to the reference beam velocity (corresponding to a 10-GeV beam with A_b=210); (e) focal spot radius; and (f) beam current.

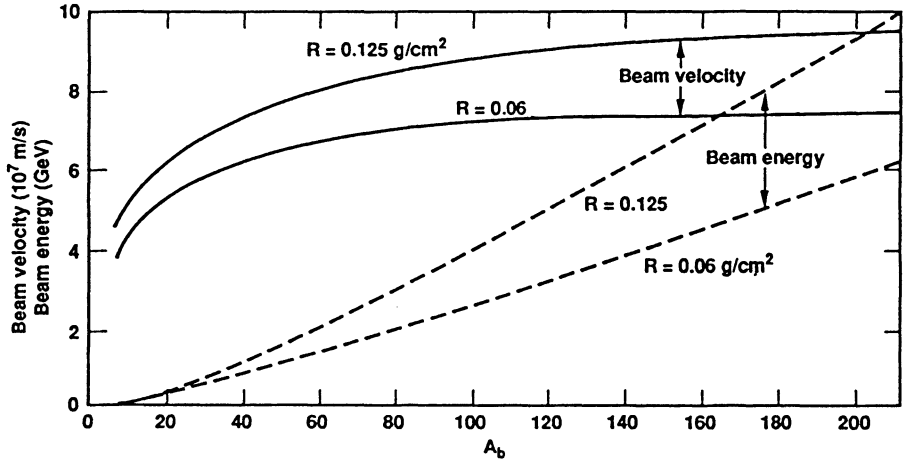

FIGURE 4: Incoming beam velocity and energy vs atomic weight for stopping ranges of 0.125 and 0.06 g/cm^2 in beryllium at 300 eV and 0.7 g/cm^3.

10% less than that for Pb, whereas the energy for Kr is about one-third that for Pb, all for $R = 0.125$ g/cm^2. Consequently, if Kr is used, the current must be about three times that of the Pb beam.

As the current and atomic weight change, the normalized emittance changes according to

$$\varepsilon_n \propto r\sqrt{\frac{T}{A_b}} \ , \tag{10}$$

where T is the transverse temperature of the ion source. If we assume that the extractor voltage and the extraction gap width of the source are fixed, then the current changes according to $I \propto r^2\sqrt{q/A_b}$, which is the maximum available current from a planar diode limited by space-charge effect, as given by the Child-Langmuir law.[13] The unnormalized emittance therefore varies as

$$\varepsilon \propto \frac{\sqrt{I}}{\beta(qA_b)^{1/4}} \tag{11}$$

if the source temperature is fixed. Using Eq. (11) and taking into account that A_b, I, and v change according to the range relation given in Fig. 4, we plot B_p vs A_b using Eq. (8) in Fig. 5. In this figure, the beam parameters are the same as those for the reference system at $A_b = 210$ with $R = 0.125$ g/cm^2. Based on the parameters of the reference system, all the beam parameters along the curves are varied according to Eq. (11) and the range relation in Fig. 4. All data in Fig. 5 correspond to focusing a beam with $q = 2$ onto a 2.5-mm-radius spot with the same beam power as for the reference system. Two cases, $R = 0.06$ and 0.125 g/cm^2, are presented. For each case, beams with no charge neutralization $I = I_0$ and with 50% neutralization in chamber $I = 0.5I_0$ are plotted. (The curves with charge neutralization are obtained simply by reducing I in Eq. (8) proportional to the amount of neutralization.) In this figure, the value of B_p corresponding to low atomic weight is less than the actual B_p because the approximation made for the logarithmic term in Eq. (2) breaks down for such beams at high currents, as mentioned earlier.

Figure 5 shows that for $R = 0.125$ g/cm^2 without charge neutralization, B_p is minimum at about $A_b = 145$. This would be the operating point to minimize B_p. For the same stopping range, beam energy decreases as A_b does. To get the same power, we must increase particle current. Hence the beam envelope at the entrance of the reactor chamber increases as A_b decreases. Consequently, if there is no need to use the lowest B_p, then one would choose large A_b to minimize the beam envelope. In any case, one would probably avoid using any ion to the left of the minimum A_b, because both B_p and beam envelope increase to the left of this point. If the maximum pole-tip field is around 5 T,[10] then the case for $R = 0.06$ g/cm^2 without charge neutralization cannot be used. One must either increase R, or introduce some charge neutralization, or increase the number of beamlets to bring the minimum B_p required to 5 T or less.

For a typical ICF reactor capsule, the power requirement is roughly 10^{13} to 10^{14} W. More than one beam is therefore needed, and this affects our estimate of the beam

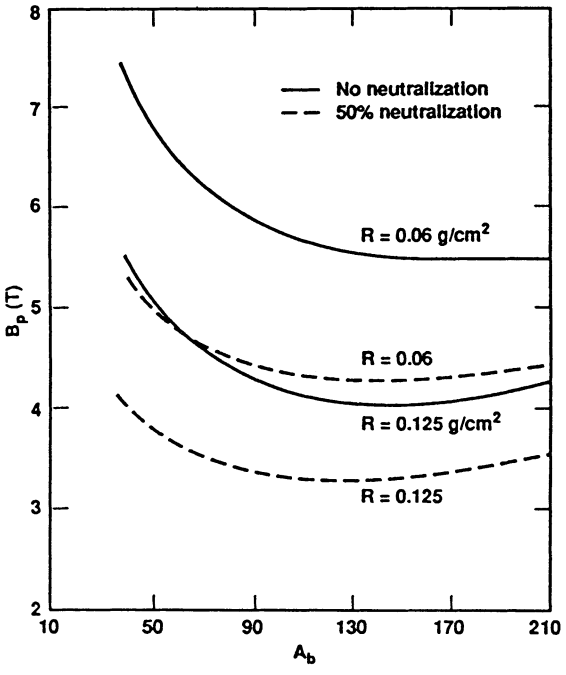

FIGURE 5: Pole-tip magnetic field vs beam atomic weight for stopping ranges of 0.125 and 0.06 g/cm^2. All data correspond to focusing a beam with q=2 onto a 2.5-mm-radius spot with the same beam power as for the reference system.

envelope size at the exit plane of the fourth quadrupole, obtained using Eq. (4). Langdon[14] has simulated multiple beam propagation in a chamber followed by focusing on a spot with 3-mm radius. In this simulation, seven beams were used. Each beam had parameters similar to those in the reference example shown here, and seven beams gave a total power of 2×10^{14} W. The simulation results showed that the effect of seven beams interacting with each other at and near the focal spot is to enlarge the beam envelope at the exit plane of the fourth quadrupole by about 15% over single-beam propagation. Thus, to estimate the multiple-beam effect on the scaling law, one can just multiply Eq. (8) by a factor of 1.15.

4. FIRST-ORDER NONDISPERSIVE FINAL-FOCUSING SYSTEM

For HIF, beam bending is necessary in the final-focusing system to avoid the direct neutron line-of-sight problem. The bending magnets must be designed so that the system is first-order nondispersive to avoid degradation in focal spot size due to momentum spread ΔP from the reference momentum P_0. The design of a first-order nondispersive system based on the reference system is presented in this section. Our emphasis is on demonstrating the feasibility of bending high-current beams, rather than on presenting a detailed engineering design.

Assuming that the bending occurs in the x plane, the single-particle equation of motion in the x direction is

$$x'' + \left(k - k_{sx} + \frac{1}{\rho^2}\right)x = -\frac{1}{\rho}\frac{\Delta P}{P_0} \quad , \tag{12}$$

where the primes represent the derivative of the quantity with respect to s, kx and $k_{sx}x$ are the quadrupole and space-charge forces per unit mass, respectively, and ρ is the radius of curvature of a particle in the magnetic field of a bending magnet. In Eq. (12), the space-charge force is linear, and this assumption is valid because the particle distribution is nearly uniform inside the envelope (except near the focal plane) as confirmed by simulations.[9] The solution to Eq. (12) is

$$x(s) = c_x(s)x_0 + s_x(s)x_0' + D(s)\Delta P/P_0 \quad , \tag{13}$$

where c_x and s_x are the solutions of the homogenous part of Eq. (12) and the subscript zero refers to initial conditions at the waist. The dispersion is given by

$$D(s) = -s_x(s_f)\int_0^{s_f}\frac{c_x}{\rho}ds + c_x(s_f)\int_0^{s_f}\frac{s_x}{\rho}ds \quad , \tag{14}$$

where s_f is the distance from the waist to the focal spot. The requirement for a first-order nondispersive system is $D = D' = 0$ at the focal spot.

To design the nondispersive system, we modify our reference system by adding three bending magnets, arranged as shown in Fig. 6(a) for a 3.3-kA beam. We then use TRACE to perform an optimization with six constraints at the focal spot. (These constraints are that the envelope sizes in the x and y directions equal the spot radius and have zero slope, and $D = D' = 0$.) Fig. 6(b) displays D and D' as functions of s. Table 3 gives the magnet strengths and the dimensions of this system.

For low-current beams, the design of a first-order nondispersive system is complete at this point. For high-current beams, however, radial electric fields generated by space charge are an important consideration in focusing. Bending magnets induce nonuniformity in the particle distribution. Consequently, nonlinear electric fields are generated; we now estimate the importance of these fields. The displacements Δx of a particle due to momentum spread is $D(\Delta P/P_0)$. Fig. 6(b) shows that the maximum value of D is 0.25 m. Thus, if we assume $\Delta P/P_0 = \pm 0.01$, the maximum Δx is ± 0.25 cm. To simplify the discussion, we assume that the beam envelope has a circular cross section. The particles having $\Delta P/P_0 = \pm 0.01$ will move a distance ± 0.25 cm from the particles with $\Delta P/P_0 = 0$, at the location where maximum Δx occurs (see Fig. 7). In Fig. 7, the electric field is nonlinear where the three circles do not overlap each other. As shown in Fig. 7, these areas have a width of $2\Delta x = 0.5$ cm. This is smaller than the envelope, which has a minor radius of about 30 cm at the location of maximum D. The nonlinear electric fields therefore affect only a small fraction of the beam particles, and this effect can therefore be ignored.

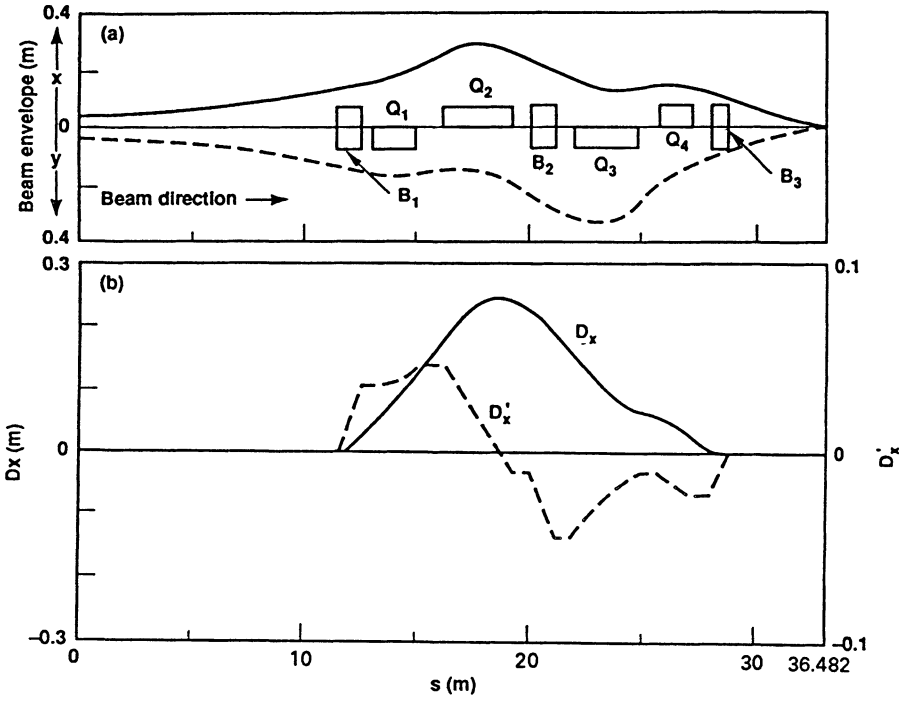

FIGURE 6: First-order nondispersive final focusing system for charge-state-2, 3.3-kA, 10-GeV beam with atomic weight 210 and unnormalized emittance 20.5 mm·mrad. (a) Layout of the system. (b) Dispersion and its derivative vs distance.

TABLE 3: System parameters with bending magnets for charge-state-2, 3-kA, 10-GeV beam with atomic weight 210 and unnormalized emittance 20.5 mm·mrad.

Quadrupole number	Magnetic field gradient (T/m)	Quadrupole length (m)	Distance from quadrupole center to waist at entrance (m)
Q_1	-6.5282	2.075	15.3415
Q_2	8.3625	3.250	19.3040
Q_3	-10.6399	3.250	25.5953
Q_4	17.0689	1.575	29.0078
Bending magnet number	**Bending angle (deg)**	**Radius of curvature(m)**	**Distance from bending magnet center to the waist at entrance (m)**
B_1	2.0000	35.2	13.1895
B_2	-1.9798	35.2	22.4622
B_3	1.2807	35.2	31.0887

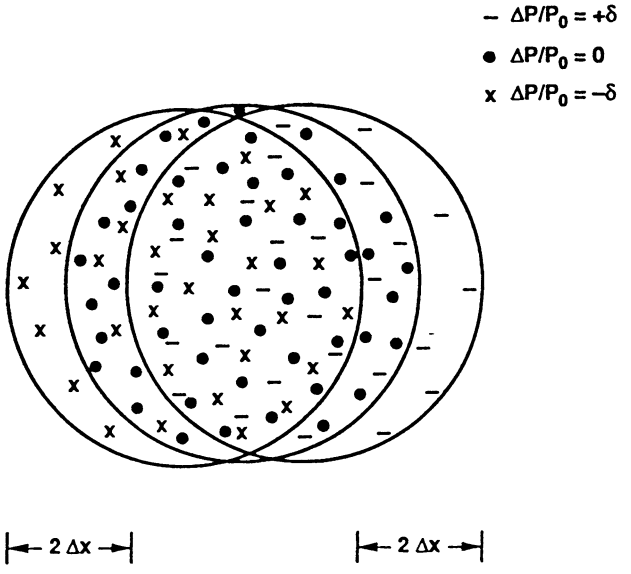

FIGURE 7: Schematic of the envelopes of particles with $\Delta P/P_0 = +\delta$, 0, and $-\delta$ at the location where maximum dispersion occurs. The nonlinear electric field occurs in the regions of width $2\Delta x$.

5. CONCLUSION

We have derived a scaling law for final focusing systems for high-current heavy-ion beams. This scaling law is useful in heavy-ion fusion system studies. For non-neutralized beams, it shows that if the beam power on the focal spot is kept fixed, the pole-tip magnetic field increases as the particle mass increases and decreases as the charge state and kinetic energy increase. If the ion range is fixed, the relation between pole-tip field and beam atomic weight can be obtained from the scaling law. Using this relation, together with other information, the most appropriate beam atomic weight can be determined. We have presented the design of a first-order nondispersive focusing system, with space-charge effect properly included. This system can avoid the direct neutron line-of-sight problem. Calculations show that the nonlinear space-charge electric field induced by the bending magnets is insignificant. In principle, a nondispersive system can therefore be designed for bending high-current beams so that direct line-of-sight neutrons can be avoided.

ACKNOWLEDGEMENTS

We thank E. P. Lee, D. S. Bailey, I. Haber, D. W. Hewett, A. B. Langdon, J. D. Lindl, R. W. Moir, and S. Yu for constructive discussions. We are grateful to P. W. Murphy for editing the manuscript. Work performed under the auspices of the U. S. Department

of Energy by the Lawrence Livermore National Laboratory under contract number W-7405-ENG-48 and by AccSys Technology under SBIR contract number DEAC03-89ER80768.

REFERENCES

1. C. Rubbia, "Inertial fusion: A contribution of accelerator technology to the energy problem?" in Proceedings of the 3rd European Particle Accelerator Conference. (Berlin, 1992), T. J. Fessenden and A. Friedman, *Nucl. Fusion* **31**, 1567 (1991).
2. D. J. Dudjiak and W. B. Hermannsfeldt, *Heavy Ion Inertial Fusion*, Amer. Inst. of Phys. Conf. Proc. **152**, edited by M. Reiser, T. Godlove, and R. O. Bangerter (Washington DC, USA, 1986), p. 111.
3. J. Hovingh, V. O. Brady, A. Faltens, D. Keefe, and E. P. Lee, *Fusion Technology* **13**, 255 (1988).
4. A. A. Garren, *ERDA Summer Study of Heavy Ions for Inertial Fusion*, R. O. Bangerter, W. B. Hermannsfeldt, D. J. Judd, and L. Smith, editors, Lawrence Berkeley Laboratory report, LBL-5543 (1976), p. 102.
5. E. P. Lee, Lawrence Berkeley Laboratory technical note HIFAN-309.
6. *HIBALL-II, An Improved Conceptual Heavy Ion Beam Driven Fusion Reactor Study*, Kernforschungszentrum Karlsruhe report KfK3840 (1985), p. 58.
7. D. D.-M. Ho, S. T. Brandon, and E. P. Lee, *Part. Accel.* **35**, 15 (1991).
8. K. R. Crandall, Los Alamos National Laboratory report LA-11054-MS (1987).
9. D. D.-M. Ho, I. Haber, K. R. Crandall, and S. T. Brandon, *Part. Accel.* **36**, 141 (1991).
10. R. W. Moir, Lawrence Livermore National Laboratory, personal communication (1991).
11. E. P. Lee, T. J. Fessenden, and L. J. Laslett, *IEEE Trans. Nucl. Sci.* **32**, 2489 (1985).
12. D. D.-M. Ho, J. D. Lindl, and M. Tabak, "Radiation converter physics for heavy-ion fusion," submitted to Nucl. Fusion.
13. J. D. Lawson, *The Physics of Charged-particle Beams* (Clarendon Press, Oxford 1977); D. W. Hewett, M. R. Gibbons, and H. L. Rutkowski, "Extracting low emittance ion beams through a switch mesh," paper forthcoming.
14. A. B. Langdon, "Chamber Propagation," *Part. Accel.* (in press).
15. J. D. Jackson, *Classical Electrodynamics*, Ch. 13 (Wiley, New York, 1975).
16. R. O. Bangerter, in *Laser Interaction and Related Plasma Phenomena*, Vol. 6, H. Hora and G. H. Miley, editors (Plenum Press, New York, 1984), p. 1013.
17. M. D. Brown and C. D. Moak, *Phys. Rev.* **86**, 90 (1972).
18. C. Deutsch, *Ann. Phys. (Paris)* **11**, 1 (1986).

APPENDIX: ION-STOPPING FORMULA

We define $\zeta \equiv \rho s$, where ρ is the density; all units in this appendix are cgs. The ion range R in g/cm^2 is then given by

$$R = \int_0^{E_0} \left(\frac{dE}{d\zeta}\right)^{-1} dE \ , \tag{A.1}$$

where E_0 is the energy of the incoming ion. The rate of energy loss with respect to ζ is [15,16]

$$\frac{dE}{d\zeta} = \frac{4\pi e^4}{A_T m_p m_e v^2} Z_{\text{eff}}^2 \left[(Z_T - \bar{Z}) \ln \Lambda_B + \bar{Z}\, G(v/v_e) \ln\, \Lambda_F \right] \ . \tag{A.2}$$

Here m_e is the electron mass, v_e is the electron thermal velocity, and the function $G(x) = \text{erf}(x) - x\text{erf}'(x)$, where $\text{erf}(x)$ is the usual error function. The target material has atomic weight A_T, atomic number Z_T, and average ionization $\bar{Z}$. The beam ions have velocity v and effective charge Z_{eff}, which, for cold matter, has the form[17]

$$Z_{\text{eff}} = Z\left[1 - 1.034 \exp\left(-4.57 \times 10^9 v Z^{-0.688}\right)\right] \ , \tag{A.3}$$

where Z is the atomic number for the beam ions. For beam ions whose velocity is high with respect to that of target electrons, Eq. (A.3) should give a reasonable approximation to Z_{eff} for hot matter. The expression for Λ_B is

$$\Lambda_B = 2m_e v^2 / I_a \ , \tag{A.4}$$

where I_a is a geometric average of the effective excitation and ionization potentials of the bound electrons and is given approximately by $10 Z_T$ eV.[18] The expression for Λ_F is

$$\Lambda_F \approx m_e v^2 / \hbar \omega_p \ , \tag{A.5}$$

where ω_p is the plasma frequency.

If beryllium is used as target material at a density of 0.7 g/cm^3 and a temperature of 300 eV, we have $2m_e v^2 / I_{av} \approx m_e v^2 / 2\hbar\omega_p$. This is why the decrease of the range of the incoming ions as the temperature of the target material rises is less important for low-Z than for high-Z material. At 300 eV, $Z_T \approx \bar{Z}$ for beryllium, and thus the term proportional to $\ln \Lambda_B$ can be ignored. Eq. (A.1) then becomes

$$R \cong 3.0 \times 10^{-2} \frac{A_b}{Z^2} \int_1^{x_0} x^3 \left[1 - 1.034 \exp(-4.7 x Z^{-0.688})\right]^{-2} \left[\bar{Z} G(x) \ln 26.8 x^2\right]^{-1} dx \ , \tag{A.6}$$

where $x \equiv v/v_e$ and $x_0 \equiv v_0/v_e$, with v_0 the initial beam velocity. In evaluating the above integral, we get $G(x) = 1$ for $x > 1$. Note that the contribution from $x < 1$ is smaller than that from $x > 1$, if the initial velocity of the ion is much greater than v_e; hence, the contribution to R from $x < 1$ can be ignored.